

Residual Stress Measurement and Calibration for A7N01 Aluminum Alloy Welded Joints by Using Longitudinal Critically Refracted (LCR) Wave Transmission Method

Qimeng Zhu, Jia Chen, Guoqing Gou, Hui Chen, Peng Li, and W. Gao

(Submitted February 1, 2016; in revised form June 8, 2016; published online August 22, 2016)

Residual stress measurement and control are highly important for the safety of structures of high-speed trains, which is critical for the structure design. The longitudinal critically refracted wave technology is the most widely used method in measuring residual stress with ultrasonic method, but its accuracy is strongly related to the test parameters, namely the flight time at the free-stress condition (t_0), stress coefficient (K), and initial stress (σ_0) of the measured materials. The difference of microstructure in the weld zone, heat affected zone, and base metal (BM) results in the divergence of experimental parameters. However, the majority of researchers use the BM parameters to determine the residual stress in other zones and ignore the initial stress (σ_0) in calibration samples. Therefore, the measured residual stress in different zones is often high in errors and may result in the miscalculation of the safe design of important structures. A serious problem in the ultrasonic estimation of residual stresses requires separation between the microstructure and the acoustoelastic effects. In this paper, the effects of initial stress and microstructure on stress coefficient K and flight time t_0 at free-stress conditions have been studied. The residual stress with or without different corrections was investigated. The results indicated that the residual stresses obtained with correction are more accurate for structure design.

Keywords A7N01 aluminum alloy welded joints, flight time at free-stress condition (t_0), initial stress (σ_0), longitudinal critically refracted wave (LCR), residual stress measurement, stress coefficient (K)

1. Introduction

The residual stress combined with external stress in a structure can be either beneficial or detrimental to the structure. Due to the detrimental effects of residual stress, including warping deformation stress corrosion cracking, and premature fatigue failure (Ref 1-7), it is highly important to consider residual stress during designing and fabricating the structure of high-speed train (Ref 7). If the residual stress results are higher than the critical value of stress, the designer has to take into consideration whether it affected the safety life of the structures.

Various methods have been used to measure the residual stress in structures. The hole-drilling method, which can be carried out with standard test procedures, is highly accurate, but the test is destructive and irreversible (Ref 8). The x-ray diffraction method requires the testing materials with crystal structure, relatively fine grain size, and could produce diffraction for any orientations from the sample surface, but the

measurable depth of x-ray diffraction is limited by tens of micrometers (Ref 9, 10).

The advantages of the LCR wave transmission method include that it is convenient to use, quick, portable, inexpensive, and free of radiation hazards. Therefore, it becomes the most popular method of ultrasonic testing for residual stress measurement. It is necessary to get the stress coefficient K and flight time (t_0) at free-stress conditions for the materials needed to be measured by correction. However, ultrasonic wave transmission method was rather sensitive to the microstructure effects, including grain size (Ref 11-13), texture (Ref 14, 15), and structure (Ref 16, 17). For high-speed trains, the main structures are manufactured by welding. Research showed that the grain size and microstructure were different in BM, HAZ, and WZ of the welded joints (Ref 18-20). When the residual stress of the different welded zones are measured only using the same parameters (e.g., K and t_0 of BM), significant error would occur and may cause incorrect safety arrangement. There has been little research on the accurate K and t_0 studies in different zones, especially to the aluminum alloy welded joints.

In this paper, the parameters of K and t_0 in WZ, HAZ, and BM are separately tested. The initial residual stress (σ_0) in calibrations samples is also reported. The samples are welded joints of 13-mm-thick A7N01 Al plate with T4 aging condition processed by MIG welding.

2. Materials and Experiments

2.1 Theoretical Background

Within the elastic limit, ultrasonic stress evaluating technique relies on the linear relationship between the stress and sound wave travel time, i.e., the acoustoelastic effect (Ref 21,

Qimeng Zhu, Guoqing Gou, and Hui Chen, School of Materials Science and Engineering, Southwest Jiaotong University, Chengdu, China; Jia Chen, School of Materials Science and Engineering, Southwest Jiaotong University, Chengdu, China and Chengdu Industry and Trade College, Chengdu, China; Peng Li, CSR Qingdao Sifang Co. Ltd, Qingdao, China; and W. Gao, Department of Chemical and Materials Engineering, The University of Auckland, PB 92019, Auckland 1142, New Zealand. Contact e-mail: gougouqing@swjtu.cn.

22). The sensitivity of ultrasonic waves to the strain has been established by Egle and Bray (Ref 21) in tensile and compressive load tests for rail steel. They proved that the sensitivity of LCR waves to the strain is higher than that of the other types of ultrasonic waves. The longitudinal critically refracted (LCR) wave propagates parallel to the surface in certain depth, as shown in Fig. 1. The first critical angle can be calculated with the following equation:

$$\theta_{LCR} = \sin^{-1}(V_1/V_2) \quad (\text{Eq 1})$$

where V_1 and V_2 are the propagating velocity in media 1 and 2, θ_{LCR} is the first critical angle ($^\circ$), θ_s is the shear angle of refraction ($^\circ$), and θ_L is the longitudinal wave angle of refraction ($^\circ$).

The velocities of the longitudinal plane waves traveling parallel to load can be related to the strain (α) by the following equations (Ref 21):

$$\rho_0 V_{11}^2 = \lambda + 2\mu + (2l + \lambda)\theta + (4m + 4\lambda + 10\mu)\alpha_1 \quad (\text{Eq 2})$$

where V_{11} is the velocity of waves in the direction of media 1 with particle displacement in the direction of media 1; ρ_0 is the initial density of material without stress λ , μ is the second-order elastic constants (Lame's constants); l , m , and n are the third-order elastic constants; α_1 , α_2 , α_3 are the components of the homogeneous triaxial principal strains; and $\theta = \alpha_1 + \alpha_2 + \alpha_3$. When the stress is in uniaxial status, $\alpha_1 = \varepsilon$, $\alpha_2 = \alpha_3 = -\mu \times \varepsilon$, where ε is the strain in the direction 1, and ν is the Poisson's ratio.

Equation 2 can be transformed into the following form using these values:

$$\rho_0 V_{11}^2 = \lambda + \mu + \left[4(\lambda + 2\mu) + 2(\mu + 2m) + \nu\mu \left(1 + \frac{2\lambda}{\mu} \right) \right] \cdot \varepsilon \quad (\text{Eq 3})$$

The variation of the velocity with the strain representing the relative sensitivity can be calculated by Eq 4. In this equation, L_{11} is the dimensionless acoustoelastic constant for LCR waves:

$$\frac{dV_{11}/V_{11}}{d\varepsilon} = 2 + \frac{(\mu + 2m) + \nu\mu(1 + 2l/\lambda)}{\lambda + 2\mu} = L_{11} \quad (\text{Eq 4})$$

However, the LCR wave is more sensitive than other types of waves, so the LCR wave was chosen to measure residual stress. L_{11} can be calculated according to Eq 4; then, we can use Eq 5 to determine the relationship between the stress variation and LCR wave velocity in the corresponding materials:

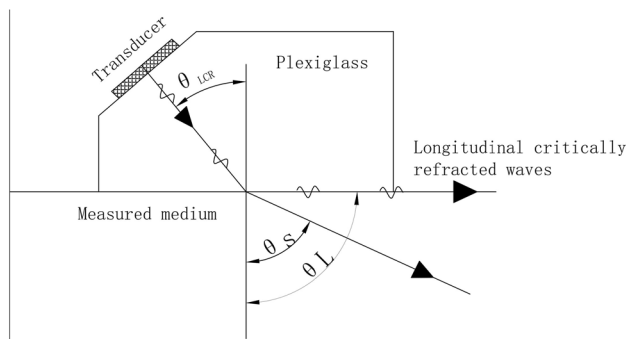


Fig. 1 Sketch to show the longitudinal critical refracted (LCR) waves

$$d\sigma = \frac{E(dV_{11}/V_{11})}{L_{11}} = \frac{E}{L_{11}t_0} dt \quad (\text{Eq 5})$$

where $d\sigma$ is the stress variation (MPa), E is the elasticity modulus (MPa), and dt is the stress variation in terms of flight time.

From Eq 5, it can be concluded that E , L_{11} , and t_0 are determined by the nature of the material itself. If we use k to represent E/L_{11} , we just need to get k by tensile experiment to measure the residual stress as shown in Eq 6:

$$\Delta\sigma = k \frac{(t - t_0)}{t_0} \quad (\text{Eq 6})$$

where t is the ultrasonic wave flight time in test samples, and t_0 is the ultrasonic wave flight time at free-stress conditions.

Actually, the distance L between the ultrasonic excitation and receiving transducer is usually fixed. The LCR wave propagate time (t) can be used to represent the LCR wave propagate velocity in the test and free-stress samples.

It is assumed that K represents k/t_0 , and Eq 6 can be simplified to Eq 7, K is called stress coefficient with the unit of MPa/ns:

$$\Delta\sigma = K\Delta t \quad (\text{Eq 7})$$

where $\Delta\sigma$ is the observed change in applied stress (MPa); Δt is LCR wave time-of-flight varying in the test samples.

2.2 Materials and Welding Parameters

A7N01P Al alloy plates with the dimension of $500 \times 300 \times 13$ mm under T4 aging condition (solution treated and naturally aged according to ISO 2107:2007) were used in this study. Joints were processed by the metal inert gas (MIG) technique with a Kemppi arc pulse 450 welding machine, and the welding direction was parallel to the rolling direction of the base metals. The welding wires are ER5356 (1.6 mm diameter). The chemical content of the base metal A7N01P and welding wire are listed in Table 1. The parameters of the welding process are listed in Table 2. The mechanical properties of A7N01P and ER5356 are listed in Table 3. In order to remove the oxides and decrease the porosity of the joint, the surface of the matrix was chemically cleaned before welding.

2.3 Hardness Testing and Microstructure Examination

Hardness was measured on a Vickers hardness (HV-10B) tester according to the ISO standard 6507-1:2005. The load was 29.4 N and lasted for 10 s. The tested zone includes BM, HAZ1, HAZ2, and WZ. The different zone was determined by microstructure examination and hardness testing.

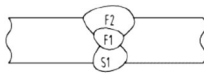
The hardness distribution is shown in Fig. 2, indicating that the base metal has the highest hardness (from 117 to 119 HV), and the hardness decreased significantly from HAZ1 (102-110 HV) to HAZ2 (88-109 HV). The weld zone had the lowest hardness (74-97 HV). Equiaxed dendrites with some porosity were distributed in WZ and fibrous tissue-like structure was in HAZ1, HAZ2, and BM zones. While the grain's size in HAZ1 zone was the largest, the grains in HAZ2 zone were larger than those in BM zone.

Table 1 Chemical composition of parent material A7N01P alloy and ER5356 welding wire (wt.%)

Materials	Chemical content, wt.%									
	Zn	Mg	Cu	Mn	Cr	Ti	Zr	Si	Fe	Al
A7N011	4.60	1.20	0.10	0.15	0.20	...	0.122	0.35	0.100	Bal.
JISH4000-20062	4.0-5.0	1.0-2.0	<0.2	0.2-0.7	<0.30	<0.20	<0.25	<0.3	<0.35	Bal.
ER5356	≤ 0.10	4.5-5.5	≤ 0.10	0.05-0.20	0.05-0.20	0.06-0.2	...	≤ 0.25	≤ 0.10	Bal.

1. A7N01—the base Al alloy employed in the present investigation
2. JISH 4000-2006—the corresponding Japanese Al alloy, the chemistry of which is detailed in Japanese Industrial Standard (JISH 4000-2006)
3. ER5356—the welding wire material used in the present research

Table 2 Welding processing parameters

Weld	Current, A	Voltage, V	Speed, cm/min	Schematic sequence
F1	210-220	23	50-60	
F2	220-230	25	40-50	
S1	220-230	23	40-50	

2.4 HAZ Microstructures Reproduction and Correction Samples Preparation

In order to obtain different zones for corrections, the welding thermal cycle test was conducted to get accurate parameters. The distribution map of the tested points is shown in Fig. 3. The measured points were perpendicular to the weld center with distances of 12.5, 22, and 45 mm separately. From the hardness and micrographs, the microstructure in the zone of 12.5 mm to the weld center can be defined as the HAZ1, the area in the zone of 22 mm to the weld center can be defined as the HAZ2, and the position in the 45 mm can be defined as the BM.

The thermal physical properties test was conducted with Gleeble 3500 thermal simulation machine. Original A7N01P-T4 alloy was fabricated for BM and HAZ samples, two for each BM, HAZ1, and HAZ2 samples. The longitudinal directions of the samples are parallel to the rolling direction. Among the two samples, one was used to measure initial stress (σ_0) by sectioning technique, and the other was used to obtain stress coefficient K and the flight time t_0 of free-stress samples. The WZ samples were obtained from the weld plates directly. Figure 3 shows the sample cutting layout.

2.5 Residual Stress Measurement

Figure 4 shows the residual stress measurement sketch with the use of *LCR* wave method. The main components were composed of (1) a data-processing computer, (2) a digital oscilloscope with the sampling frequency of 5 GHz, (3) an ultrasonic synchronous signal generator, and (4) an excitation and receiving transducer with temperature sensor.

LCR wave transmission velocity is affected by the testing temperature, so it must be calibrated with a temperature sensor. In this study, the frequency of transducers was 4 MHz with the diameter of 6.8 mm. The measured depth of the Al samples was about 2 mm, a measurement equal to the depth measured by the

hole-drilling method. The distance between the excitation and receiving transducer was 30 mm. The inclination angle between the transducer and measured plane was 28.1° , and the error of time measurement was ± 0.5 s.

2.6 *LCR* Wave Flight Time (t_0) and Initial Stress (σ_0) in Free-Stress Samples

The microstructure of A7N01P alloy is changed at about 180°C , so the annealing cannot be used to eliminate the residual stress for making free-stress calibration samples of Al alloys. In this study, the calibration samples were prepared by line cutting with a width of 25 mm. The initial residual stress of different zones' calibration samples were measured by sectioning.

The *LCR* wave was used to measure the flight time (t_0) at “free-stress” conditions in WZ, HAZ1, HAZ2, and BM. In this paper, it assumes that the initial residual stress state of calibration samples were the same as the cut samples. The *LCR* wave spread in a wide field making it difficult to determine the exact location of the emitted points, and it is also difficult to measure the exact t_0 in the calibration samples. We assume t_0 of BM was 0, and the device shown in Fig. 4 was used to measure t_0 of the other zones

2.7 Correction of Stress Coefficient K

The reproduced calibration samples were used to calibrate K in different zones. The calibration procedure was processed following the ASTM B557-10 standard as shown in Fig. 5. The Plexiglas wedge with fixing ultrasonic transducers was attached on the calibration samples. The direction of the *LCR* wave transmission was parallel to the direction of residual stress measurement. The tensile correction samples were fixed on the stretching machine DNS300; the steady applied load was about $2\text{ kN} \pm 150\text{ N}$ and kept for 20 min. When the external load stress reached 70% of the yield strength of samples, the calibration procedure was ended.

2.8 *LCR* Wave Transmission Method Used for Residual Stress Measurement in Welded Joints

The welded joints' residual stress was measured with the *LCR* wave transmission method. The measured zones and points distribution are shown in Fig. 6. To obtain accurate results, the reinforcement was polished, and the widths were 20, 18, 12, and 100 mm in WZ, HAZ1, HAZ2, and BM, respectively. The measured direction was parallel to the weld, and the increment between each point was 2 mm in WZ, HAZ1, and HAZ1, and 10 mm in BM. Hole-drilling method was employed to validate the *LCR* wave method (Fig. 6).

3. Results and Discussion

3.1 The Effect of Microstructure on the Stress Coefficient K

The WZ zone has the cast microstructure with a mixture of filler materials and BM materials. If the K value was not calibrated in each zone and only used the same K value (e.g., the K value of BM), it may produce errors in each zone. According to Eq 7, the reciprocal slopes of lines were stress coefficient K as shown in Fig. 7. The stress coefficient K in each zone is listed in Table 4. Comparing the measured results

with the K value of BM, it can be found that the value of the WZ zone was 31% higher than the BM zone. But in HAZ1 and HAZ2, the errors were only 7 and 4%, according to Eq 8 as listed in Table 5. Equation 9 was used to correct the error resulted from K .

$$\text{Errors} = (K_{(WZ,HAZ1,HAZ2)} - K_{BM})/K_{BM} \quad (\text{Eq 8})$$

$$\sigma_{(WZ,HAZ1,HAZ2,BM)} = K_{(WZ,HAZ1,HAZ2,BM)}(t - t_0) \quad (\text{Eq 9})$$

where $K_{(WZ, HAZ1, HAZ2, BM)}$ is the stress coefficient K of WZ, HAZ1, HAZ2, and BM.

Table 3 Mechanical properties of A7N01P and ER5356

Material	Tensile strength, σ_b /MPa	Yield strength, $\sigma_{0.2}$ /MPa	Elongation, δ /%
A7N01	365	295	12
ER5356	265	120	26

3.2 Microstructure Effect on Flight Time at Free-Stress Conditions (t_0)

The flight time in the “free-stress” calibration samples is listed in Table 6. The different microstructures in each zone also had a great effect on the flight time (t_0) at the “free-stress” calibration samples. The largest difference of t_0 was in WZ for

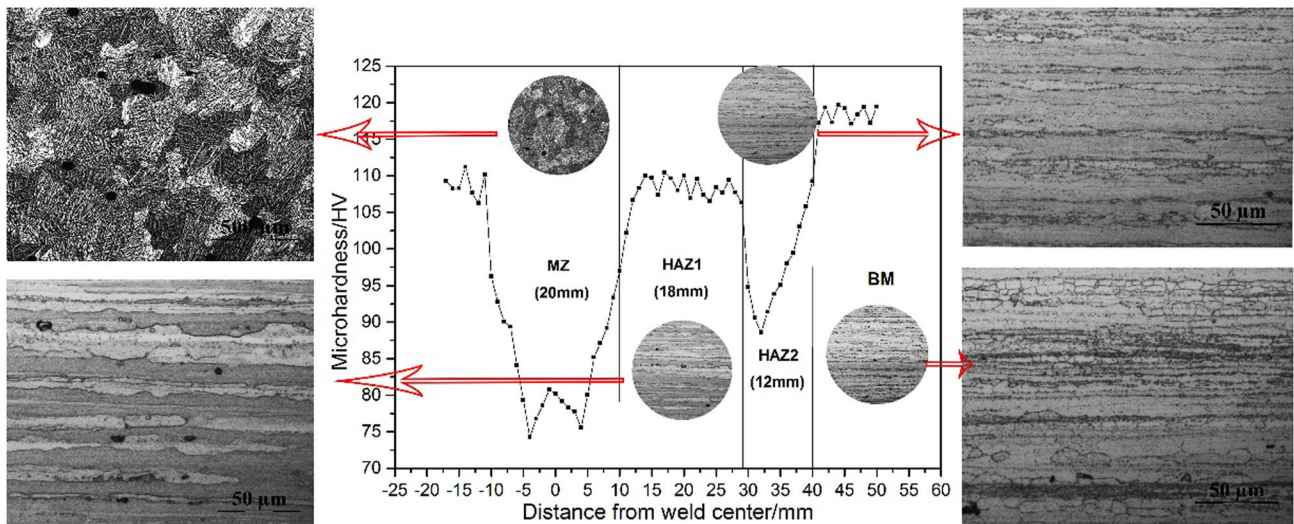


Fig. 2 Hardness and microstructure distribution from weld zone to base metal

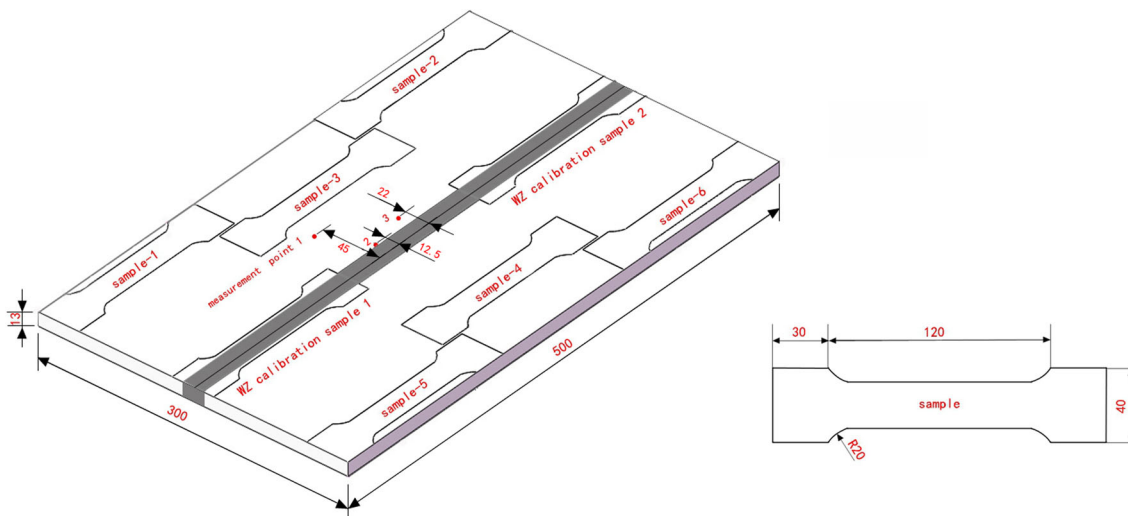


Fig. 3 Thermal cycling tested points and samples for reproducing microstructure in each zone

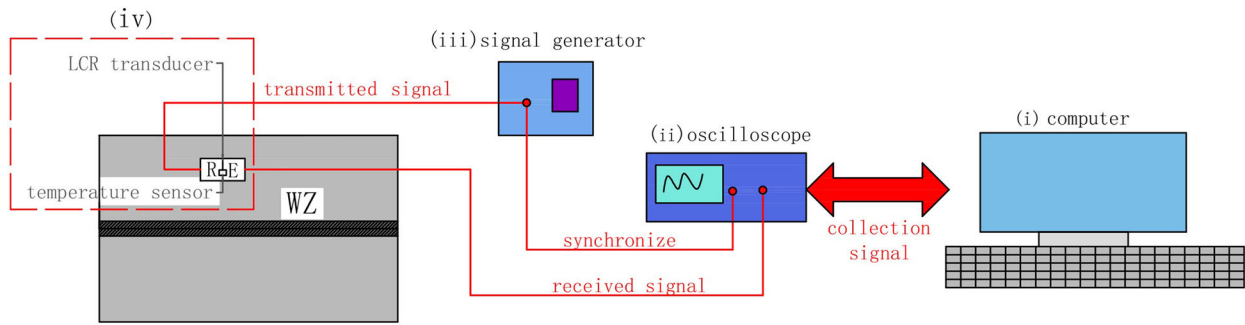


Fig. 4 Sketch of the ultrasonic residual stress measurement system

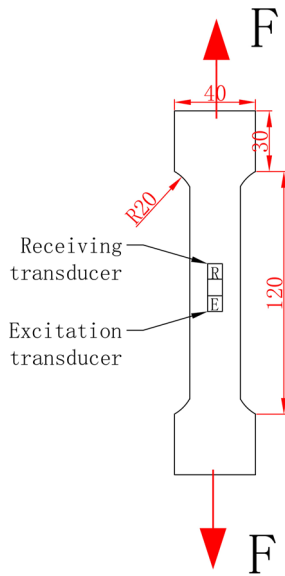


Fig. 5 Sketch of tensile calibration

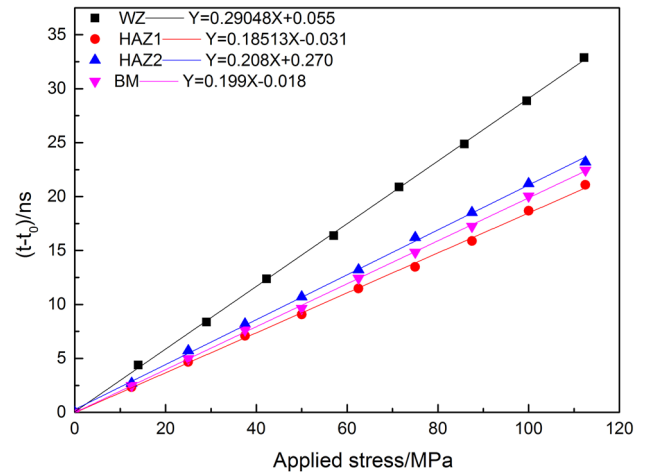


Fig. 7 Influence of microstructure on the acoustoelastic correction coefficient

Table 4 Stress coefficient K with initial stress

Zones	Weld	HAZ1	HAZ2	BM
K	3.44	5.40	4.81	5.03

Table 5 Percentage error resulting from using K from BM

Zones	WZ	HAZ1	HAZ2	BM
Percentage error, %	31	7	4	0

Table 6 Flight time t_0 in “free-stress” samples

Zones	WZ	HAZ1	HAZ2	BM
Time-of-flight relative to BM, ns	8.5	6.5	5.0	0

Table 7 Errors resulted from using t_0 in BM to determine the residual stress in other zones (MPa)

Regions	WZ	HAZ1	HAZ2	BM
Errors, MPa	42.76	32.70	25.15	0

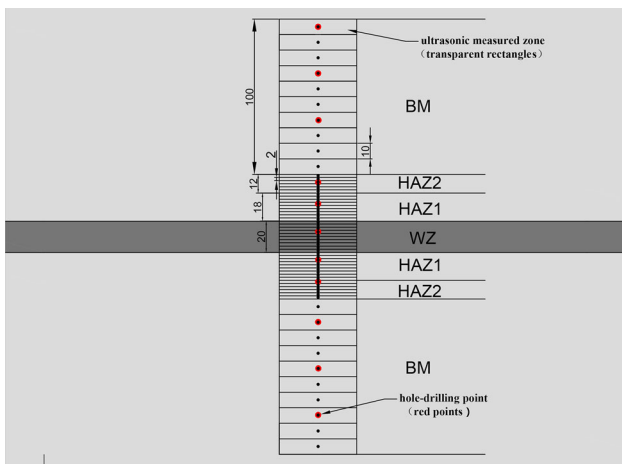


Fig. 6 Testing points and zones distribution diagram

the different microstructures. From Table 6, it can be seen that the LCR wave velocity became much slower with the distance closer to the weld center.

The grain size and precipitates both affected the *LCR* wave velocity. The errors produced by using the t_0 of BM to measure the residual stress in other zones were calculated by Eq 10 as listed in Table 7. Equation 11 was used to determine the residual stress in different zones with the correction of t_0 in different zones.

$$\text{Errors} = t_{(WZ,HAZ1,HAZ2)} \times K_{BM} \quad (\text{Eq 10})$$

$$\sigma_{(BM,HAZ1,HAZ2,WZ)} = K(t - t_{(0BM,0AZ1,0HAZ2,0WZ)}) \quad (\text{Eq 11})$$

where $t_{(0BM,0HAZ1,0HAZ2,0WZ)}$ is the flight time in “free-stress” samples in BM, HAZ1, HAZ2, and WZ, respectively.

3.3 The Effect of Initial Stress (t_0) on Measured Results

The flight time (t_0) in “free-stress” samples of each zone are not equal to the real time without initial stress, and the initial

stress is listed in Table 8. While K depends on t_0 and the nature of material according to Eq 5-7, but the errors that come from the initial stress cannot be eliminated unless getting free-stress calibration samples. Equation 12 is for reducing the errors resulting from σ_0 .

$$\sigma_{(WZ,HAZ1,HAZ2,BM)} = K(t - t_0) + \sigma_{(0WZ,0HAZ1,0HAZ2,0BM)} \quad (\text{Eq 12})$$

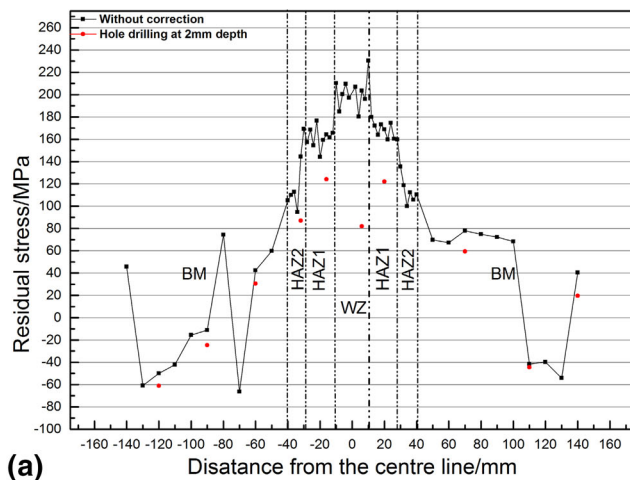
where $\sigma_{(0WZ, 0HAZ1, 0HAZ2, 0BM)}$ is the initial stress in calibration samples of WZ, HAZ1, HAZ2, and BM, respectively.

3.4 Residual Stress

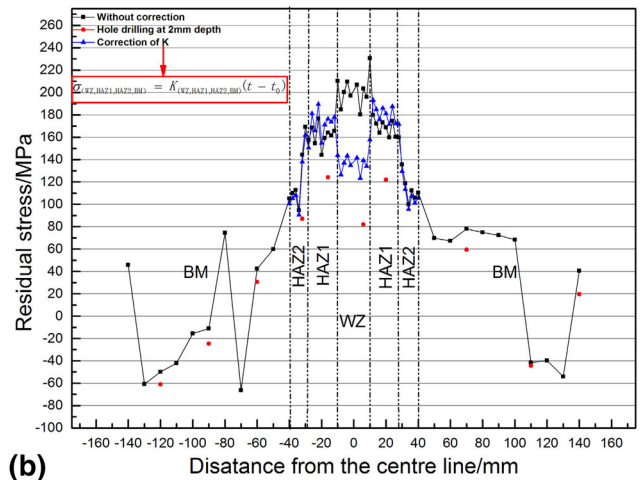
Figure 8(a-d) shows the residual stresses with different correction methods, or without correction, obtained by using *LCR* wave transmission method. The hole-drilling method was also employed for verification. As Fig. 8 shows, the results are quite different. While the residual stress decreased in HAZ2 zone using the correction of K_{HAZ2} , the residual stress increased in HAZ1 using the correction of K_{HAZ1} , and the corrected results changed significantly in WZ. The maximum corrected values of WZ, HAZ1, and HAZ2 were 72.9, -13.2, and 7.40 MPa, respectively. With the correction of K and t_0 in different zones (Fig. 8c), the results were much closer to the

Table 8 Initial residual stress σ_0 of each zone

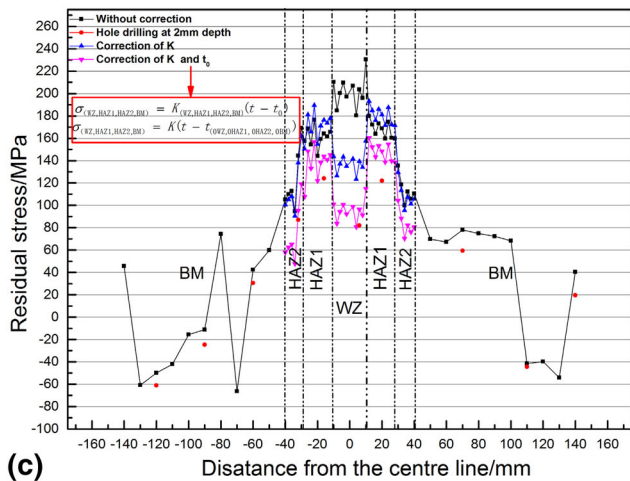
Zone	WZ	HAZ1	HAZ2	BM
Residual Stress/MPa	9.87	11.32	7.49	5.21



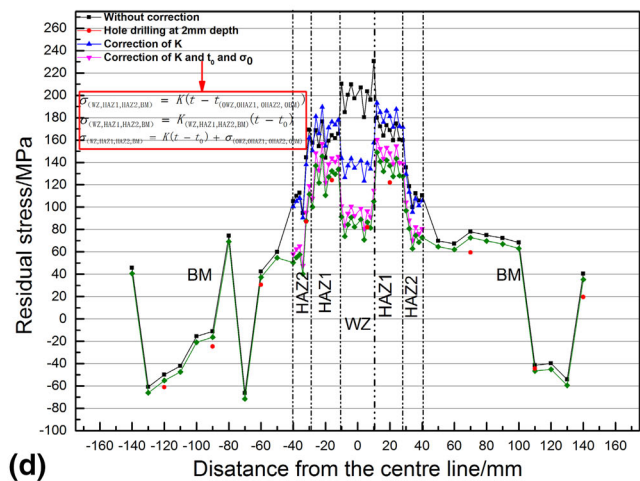
(a)



(b)



(c)



(d)

Fig. 8 Residual stress: (a) the without correction compared with hole-drilling, (b) with correction of K compared with hole-drilling, (c) with correction of K and t_0 compared with hole-drilling, and (d) with correction of K , t_0 and σ_0 compared with hole-drilling

hole-drilling tested results. The largest deviations from the hole-drilling method were 18.5, 26.4, and 8.22 MPa in WZ, HAZ1, and HAZ2, respectively. The difference in WZ became

smoother. The corrected values were 42.8, 32.7, and 25.2 MPa in WZ, HAZ1, and HAZ2, respectively, with the correction of t_0 in each zone.

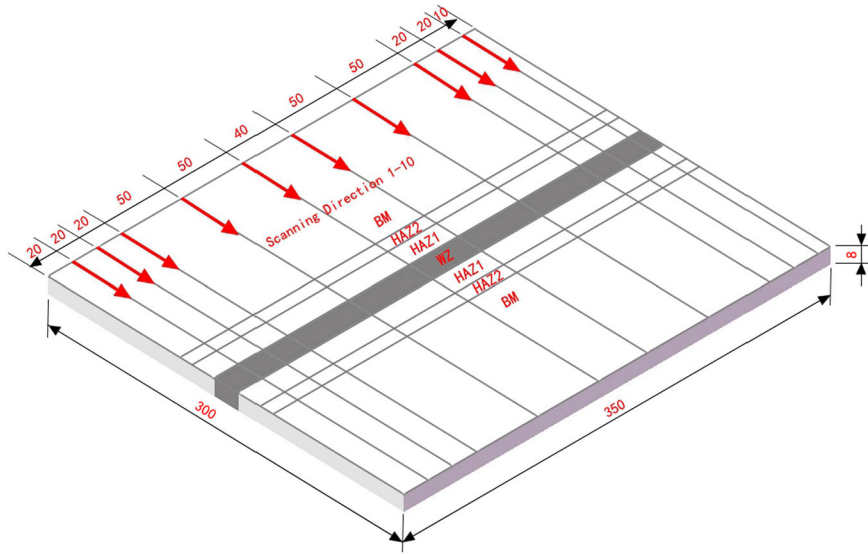


Fig. 9 LCR wave-measured zones and path distribution

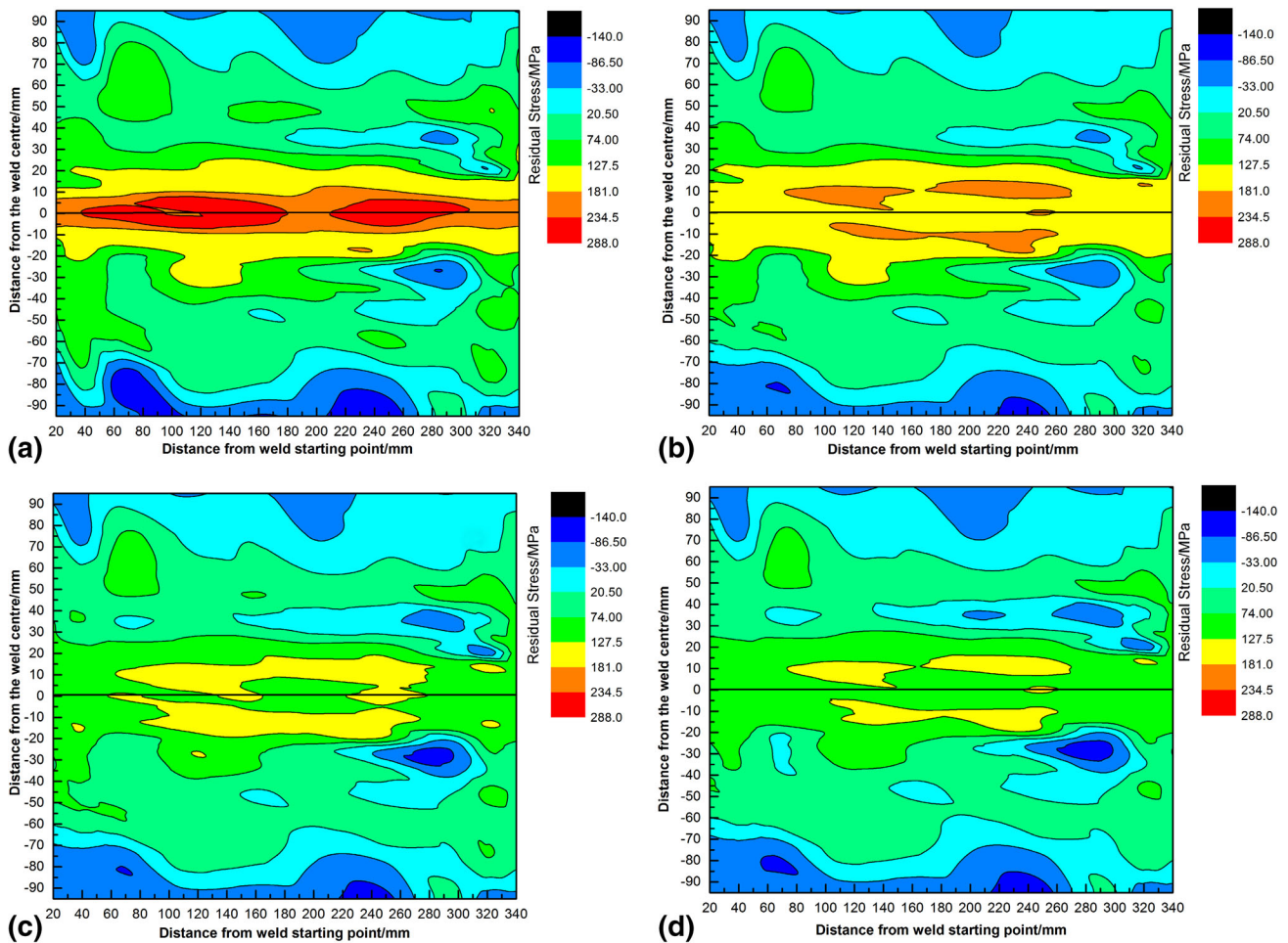


Fig. 10 LCR wave-measured contour: (a) without correction, (b) with correction of K , (c) with correction of K and t_0 , and (d) with correction of K , t_0 , and σ_0

With the correction of K , t_0 , and σ_0 in different zones (Fig. 8d), the data tested with the LCR wave method were in coincidence with the data measured by the hole-drilling method. The corrected values were 9.87, 11.3, 7.49, and 5.21 MPa in WZ, HAZ1, HAZ2, and BM, respectively, with the correction of initial stress σ_0 in each zone.

The largest deviations were 20.8, 67.3, 46.7, and 125.6 MPa in BM, HAZ2, HAZ1, and WZ, respectively, compared with hole-drilling results without any correction. However, the largest deviations of corrected results were 15.6, 10.0, 15.1, and 8.66 MPa in BM, HAZ2, HAZ1, and WZ, respectively, compared with the hole-drilling results with correction of K , t_0 , and σ_0 .

Besides, in Fig. 8(a), the LCR wave measurement results did not show double-peak state without correction, this was not consistent with the theoretical results. All values in Fig. 8(b) to (d) showed good double-peak state.

It can be seen that the microstructure difference in each zone affected the flight time (t_0) in free-stress samples and had a more significant effect on WZ stress coefficient K compared with other zones. Whether t_0 or K has a significant effect on WZ measured results, t_0 has a much stronger effect on HAZ1, HAZ2, and BM than K . The errors produced by initial stress (σ_0) were relatively stable in all zones, about 10 MPa.

An A7N01P welded plate with the dimension of $350 \times 300 \times 8$ mm was measured by LCR wave transmission method as shown in Fig. 9. The results with and without correction are shown in Fig. 10.

As shown in Fig. 10(a), the peak values without correction were 281 MPa, which was close to the weld yield strength 295 MPa with reinforcement. The double peak appeared after the correction of K as shown in Fig. 10(b). The peak values with correction of K were about 201 MPa. The residual stress trend did not have significant change with the correction of t_0 and σ_0 , but the residual stress values decreased significantly in Fig. 10(c), as the peak values without correction were about 158 MPa. In Fig. 10(d), the peak value presented in HAZ is about 147 MPa with correction of K , t_0 , and σ_0 . The conclusion can be drawn that with the correction, the residual stresses were more accurate. Therefore, the designer can take it into more accurate consideration for the safety design of important structures used in high-speed trains.

4. Conclusion

Longitudinal critically refracted (LCR) wave was used to measure residual stress in Al alloy weld joints. The following conclusions can be drawn.

1. The microstructure in WZ, HAZ1, HAZ2, and BM have a significant effect on the K and t_0 , especially in WZ, it is necessarily to correct the errors resulted from different microstructure in avoid of the overestimated of residual stress.
2. The stress coefficient K with initial stress (σ_0) were 3.44, 5.40, 4.81, and 5.03 in WZ, HAZ1, HAZ2, and BM, respectively. The percentage errors resulted from using the same K of BM were 37, 4, and 9.8% in WZ, HAZ1, and HAZ2, respectively. The errors resulted from using the same t_0 of BM to determine the residual stress in other zones were 42.8, 32.7, and 25.2 MPa in WZ, HAZ1, and HAZ2, respectively.
3. The LCR wave-measured results only showed double peak after corrections; the base material A7N01P is stronger than the filler material ER5356, and the welding residual stress should show double peak theoretically, but higher K and lower t_0 of BM than that of MZ produce the peak residual stress in WZ.
4. The K , t_0 , and σ_0 all have a significant effect on the residual stress measurement results, K has more a more obvious effect in WZ and t_0 has a more obvious effect than K and σ_0 in all the measured zones.
5. To measure welding residual stress of A7N01P, t_0 , K , and σ_0 in different zones must be measured individually by using LCR wave, the correction method may be also effective for the other materials.

Acknowledgments

The data in this paper are from a few projects, including (i) Research of the key technologies and equipment for next-generation railway transportation in cities and (ii) Basic research of the design and advanced welding technology for high-speed trains in the wide region environment. The authors acknowledge financial support from the National Science and Technology Pillar Program (No. 2015BAG12B01) and National Key Basic Research and Development Plan (No. 2014CB660807).

References

1. R. Unnikrishnan, K.S. Idury, T. Ismail, A. Bhadauria, S. Shekhawat, R.K. Khatirkar, and S.G. Sapate, Effect of Heat Input on the Microstructure, Residual Stresses and Corrosion Resistance of 304L Austenitic Stainless Steel Weldments, *Mater. Charact.*, 2014, **93**, p 10–23
2. L. Basatskaia and I. Ermolov, Theoretical Study of Ultrasonic Longitudinal Subsurface Waves in Solid Media, *Sov. J. Nondestruct. Test.*, 1981, **16**, p 524–530
3. W. Baldwin, Jr., Residual Stress, *Met. Prog.*, 1955, **68**, p 89–96
4. Y. Xie, Y. Wu, J. Burns, and J. Zhang, Characterization of Stress Corrosion Cracks in Ni-Based Weld Alloys 52, 52M and 152 Grown in High-Temperature Water, *Mater. Charact.*, 2016, **112**, p 87–97
5. M. Marques, A. Ramasamy, A. Batista, J. Nobre, and A. Loureiro, Effect of Heat Treatment on Microstructure and Residual Stress Fields of a Weld Multilayer Austenitic Steel Clad, *J. Mater. Process. Technol.*, 2015, **222**, p 52–60
6. G. Gnirss, Vibration and Vibratory Stress Relief. Historical Development, Theory and Practical Application, *Weld. World*, 1988, **26**, p 284–291
7. G. Gou, M. Zhang, H. Chen, J. Chen, P. Li, and Y. Yang, Effect of Humidity on Porosity, Microstructure, and Fatigue Strength of A7N01S-T5 Aluminum Alloy Welded Joints in High-Speed Trains, *Mater. Des.*, 2015, **85**, p 309–317
8. N. Rossini, M. Dassisti, K. Benyounis, and A. Olabi, Methods of Measuring Residual Stresses in Components, *Mater. Des.*, 2012, **35**, p 572–588
9. P.S. Prevey, X-ray Diffraction Residual Stress Techniques, *ASM Int. ASM Handb.*, 1986, **10**, p 380–392
10. L. Meisner, A. Lotkov, M. Ostapenko, and E.Y. Gudimova, X-ray Diffraction Study of Residual Elastic Stress and Microstructure of Near-Surface Layers in Nickel-Titanium Alloy Irradiated with Low-Energy High-Current Electron Beams, *Appl. Surf. Sci.*, 2013, **280**, p 398–404
11. A.B. Bouda, S. Lebaili, and A. Benchaala, Grain Size Influence on Ultrasonic Velocities and Attenuation, *NDT E Int.*, 2003, **36**, p 1–5
12. W.A. Olsson, Grain Size Dependence of Yield Stress in Marble, *J. Geophys. Res. Atmos.*, 1974, **79**, p 4859–4862

13. S.M. Kumaran, Evaluation of Precipitation Reaction in 2024 Al–Cu Alloy Through Ultrasonic Parameters, *Mater. Sci. Eng. A*, 2011, **528**, p 4152–4158
14. P. Marie-Aude, E.G. Rachid, J. Moysan, G. Corneloup, and B. Chassignole, Acoustical Characterization of Austenitic Stainless Steel Welds for Experimental and Modeling NDT, *J. Adv. Sci.*, 2005, **17**, p 76–81
15. C.M. Sayers, Ultrasonic Velocities in Anisotropic Polycrystalline Aggregates, *J. Phys. D Appl. Phys.*, 2000, **15**, p 2157–2167
16. C.H. Gur and I. Cam, Comparison of Magnetic Barkhausen Noise and Ultrasonic Velocity Measurements for Microstructure Evaluation of SAE 1040 and SAE 4140 Steels, *Mater. Charact.*, 2007, **58**, p 447–454
17. Y.H. Nam, Y.I. Kim, and S.H. Nahm, Evaluation of Fracture Appearance Transition Temperature to Forged 3Cr–1Mo–0.25V Steel Using Ultrasonic Characteristics, *Mater. Lett.*, 2006, **60**, p 3577–3581
18. K. Sawada, T. Hara, M. Tabuchi, K. Kimura, and K. Kubushiro, Microstructure Characterization of Heat Affected Zone After Welding in Mod. 9Cr–1Mo Steel, *Mater. Charact.*, 2015, **101**, p 106–113
19. F. Khodabakhshi, M. Haghshenas, S. Sahraeinejad, J. Chen, B. Shalchi, J. Li, and A. Gerlich, Microstructure-Property Characterization of a Friction-Stir Welded Joint Between AA5059 Aluminum Alloy and High Density Polyethylene, *Mater. Charact.*, 2014, **98**, p 73–82
20. M.M. Amrei, H. Monajati, D. Thibault, Y. Verreman, L. Germain, and P. Bocher, Microstructure Characterization and Hardness Distribution of 13Cr4Ni Multipass Weld Metal, *Mater. Charact.*, 2016, **111**, p 128–136
21. D.M. Egle and D.E. Bray, Measurement of Acoustoelastic and Third-Order Elastic Constants for Rail Steel, *J. Acoust. Soc. Am.*, 1976, **60**, p 741–744
22. D.E. Bray, N. Pathak, and M. Srinivasan, Residual Stress Mapping in a Steam Turbine Disk Using the LCR Ultrasonic Technique, *Mater. Eval.*, 1996, **54**, p 832–839